

# Divertor Study on DEMO Reactor<sup>\*)</sup>

Kazuo HOSHINO, Nobuyuki ASAKURA, Katsuhiro SHIMIZU<sup>1)</sup>, Shinsuke TOKUNAGA, Tomonori TAKIZUKA<sup>2)</sup>, Youji SOMEYA, Makoto NAKAMURA, Hiroyasu UTOH, Yoshiteru SAKAMOTO and Kenji TOBITA

*Japan Atomic Energy Agency, Rokkasho, Aomori 039-3212, Japan*

<sup>1)</sup>*Japan Atomic Energy Agency, Naka, Ibaraki 311-0193, Japan*

<sup>2)</sup>*Osaka University, Suita, Osaka, 565-0871, Japan*

(Received 24 December 2013 / Accepted 9 April 2014)

Huge power handling in the SOL/divertor region is one of the crucial issues for a tokamak fusion reactor. Divertor design study of a DEMO reactor with fusion power of 3 GW and ITER size plasma has progressed using the integrated divertor code SONIC. Recently, to improve conversion of the solution for the DEMO divertor plasma simulation, SONIC code has been improved. The calculation time is significantly reduced by (i) the backflow model for the simplified impurity exhaust process and (ii) optimization on HELIOS at BA-IFERC. In the SONIC simulation, the partial detached divertor plasma was obtained by the Ar impurity seeding. Although the plasma heat load at the outer target was reduced by the partial detachment, the contribution of the impurity radiation and the surface recombination of the fuel ions to the target heat load became large. As a result, the peak of the total target heat load was estimated to be 16 MW/m<sup>2</sup>. In order to reduce the total heat load, control of the impurity radiation profile by kind of seeding impurity species and the divertor geometry has been studied. They can decrease the target heat load, but the peak heat load is still larger than the heat removal capability of the present divertor target concept. Further design study including change of the machine specifications is necessary.

© 2014 The Japan Society of Plasma Science and Nuclear Fusion Research

Keywords: DEMO reactor, divertor power handling, integrated divertor code, divertor plasma detachment, impurity seeding, divertor geometry effect

DOI: 10.1585/pfr.9.3403070

## 1. Introduction

Huge power handling in the SOL/divertor region is one of the crucial issues for a tokamak fusion DEMO reactor, such as SSTR [1], Demo-CREST [2], ARIES-AT [3], PPCS [4, 5], SlimCS [6, 7] and so on. In the DEMO reactor for the fusion power of 3 GW, exhausted thermal power from the core plasma to the SOL/divertor ( $P_{\text{ext}}$ ) is expected to be larger than 500 MW, which is 5-6 times larger than that in ITER. On the other hand, the desirable heat load on the divertor target is less than or comparable to the ITER design of 10 MW/m<sup>2</sup> because the available material is restricted by the strong neutron irradiation environment. For a mono-block target with tungsten and reduced activation ferritic martensitic steel as the structure and the water-cooling pipe materials, the power removal capability is evaluated to be 5-7 MW/m<sup>2</sup> [6]. The primary technique for reduction of the divertor heat load is enhancement of the radiation loss by impurity seeding.

SlimCS [6, 7] is a conceptual DEMO reactor with fusion power of 3 GW and ITER size plasma. The plasma parameters are the major radius  $R_p = 5.5$  m, the minor radius  $a_p = 2.1$  m, the plasma current  $I_p = 16.7$  MA, toroidal field  $B_t = 6.0$  T, ellipticity  $\kappa_{95} = 2.0$ , triangularity  $\delta_{95} = 0.35$ ,

and plasma volume  $V_p = 941$  m<sup>3</sup>. For the fusion power of  $P_{\text{fus}} \sim 3$  GW,  $P_{\text{ext}} \sim 500$  MW is expected. A power handling scenario has been investigated by using a suite of integrated divertor codes SONIC [8, 9], in order to produce the detachment (the electron temperature  $T_e$  less than a few eV for suppression of the target erosion) at the divertor target [10–13]. As will be discussed in section 3, SONIC simulation for the SlimCS divertor plasma with the large Ar impurity seeding shows the divertor power load is still higher than 10 MW/m<sup>2</sup>, although 92 % of  $P_{\text{ext}}$  is radiated by the Ar impurity. There are large gaps from the present experiments on development of power handling scenario in a viewpoint of both the huge exhausted power and the large impurity radiation fraction. Therefore, development of the power handling scenario is important and challenging issue in the DEMO design study and predictive simulation study has an important role.

In this paper, recent numerical study for DEMO divertor design in Japan Atomic Energy Agency (JAEA) is summarized. The integrated divertor code SONIC and recent development toward the DEMO divertor simulation are described in section 2. The DEMO divertor performance and the power handling are investigated by using SONIC, in section 3. Finally, summary is given and future issues of the DEMO divertor design and simulation are discussed in section 4.

author's e-mail: hoshino.kazuo@jaea.go.jp

<sup>\*)</sup> This article is based on the invited presentation at the 23rd International Toki Conference (ITC23).

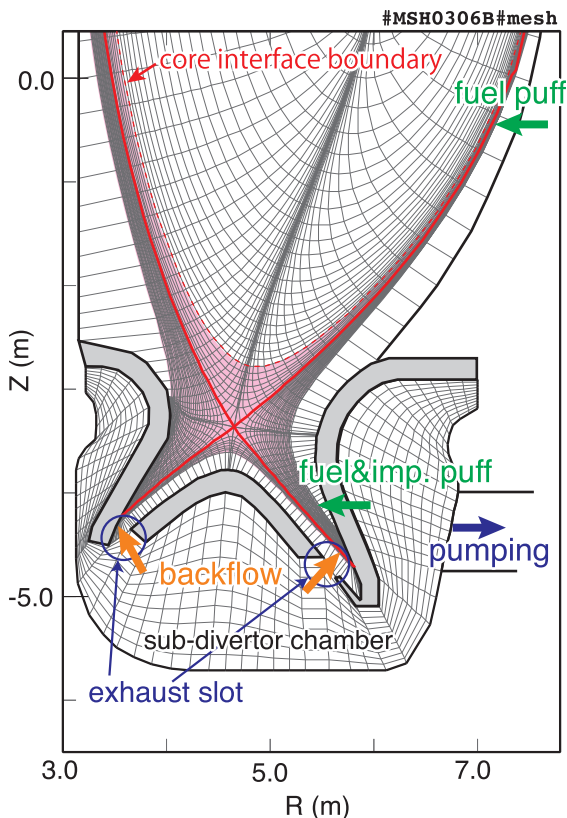


Fig. 1 Numerical grid for the SlimCS divertor simulation.

## 2. Integrated Divertor Code SONIC

In the divertor, there are complicated and non-linear interactions among fuel plasma, fuel neutral, impurity and plasma facing wall. Usually, a suitable model for each element is developed and they are integrated as a divertor code. Various divertor simulation codes, such as SOLPS [14], UEDGE [15] and so on, have been developed.

In JAEA, a suite of integrated divertor codes SONIC [8, 9] has been developed for the interpretation and prediction of the divertor plasma characteristics. The SONIC suite consists of the 2D plasma fluid code (SOLDOR), the neutral Monte-Carlo (MC) code (NEUT2D) and the impurity MC code (IMPMC).

The transport of bulk ion  $D^+$  is described in a fluid approximation by the SOLDOR code. The fluid equations of the particle conservation, parallel ion momentum conservation, and ion and electron energy conservation are solved in the SOL and divertor region on the 2D poloidal plane shown in Fig. 1. The narrow edge region ( $0.95 < r/a < 1.0$ ) is also calculated to take into account of the poloidal asymmetry in the core region. The perpendicular transport is assumed to be anomalous, while the parallel transport along field lines in the SOL region is assumed to be classical. In the present version of SOLDOR, the effects of drifts and current are neglected.

The transport of neutral atom D and molecule  $D_2$  are traced inside the whole vessel, i.e., the core plasma, SOL divertor and vacuum region including the exhaust route,

by the neutral MC particle code NEUT2D. The important atomic and molecular processes for appropriate treatment of the recycling are taken into account [8].

The MC particle code IMPMC treats the impurity transport with a guiding center approximation, while most of other divertor codes treat the impurity ion species as fluid. The MC approach has a lot of flexibility in modeling of the impurity transport, such as interactions with walls/divertor, kinetic effects and so on. On the other hand, disadvantages of the MC approach are large Monte-Carlo noise, large computer resource etc. Recently, these disadvantages have been overcome, and the IMPMC code has been self-consistently integrated with SOLDOR/NEUT2D [9]. In the present version of the SONIC, only one impurity species can be treated by IMPMC. For analysis of the synergetic effects of the multi impurity species, the non-coronal radiation model is used together. Development toward treatment of the multi impurity species by IMPMC is ongoing with development of the MPMD system described below.

### 2.1 Code development toward the DEMO divertor simulation

In the DEMO divertor simulation by using the SONIC suite, conversion of the solution is rather unstable/oscillating due to the large flux and the low temperature in the divertor and the large impurity radiation power. Recently, in order to obtain the more stable solution and then to apply the DEMO divertor simulation, the SONIC suite has been improved. Also, integration of the core transport to the SONIC suite is in progress for self-consistent analysis of the DEMO power handling scenario.

#### (i) the backflow model for simplified impurity exhaust process

In the noble impurity gas seeding simulation for DEMO, long exhaust processes for the noble gas impurity became problem. In the impurity MC calculation, trajectory of the noble gas impurity has to be traced until it is exhausted, while trace of the impurities generated from the plasma facing material by the sputtering can be finished by deposition on the wall surface. Characteristic time of the impurity gas transport, especially in the sub-divertor chamber under the dome (see Fig. 1), is long ( $> 10$  s). The long MC calculation for such exhaust processes is unreasonable for the iterative calculation of SONIC.

In order to reduce the calculation time for long impurity exhaust process, the backflow model has been developed [16]. In the full calculation including the exhaust process, trajectories of injected impurity particles are traced until all particles are exhausted, i.e., weight of test particles becomes zero. Because decrease in weight per a hit to the pumping port is only a few percent, most of the test particles go back to the plasma region through exhaust slots. Therefore they go back and forth between the plasma region and the sub-divertor chamber through the exhaust

slots. On the other hand, in the backflow model, amount of the backflow flux to the divertor region is evaluated in advance, and then simulating impurity flux injected from the exhaust slot to the divertor region like a backflow as shown in Fig. 1. In the backflow model, seeding impurities by puff and backflow flux are traced only in the plasma region because transport effect in the sub-divertor chamber is already taken into account as a backflow. By this model, the iterative calculation of SONIC becomes ten times faster and iterative calculation for DEMO divertor simulation becomes possible within a reasonable calculation time.

**(ii) optimization on HELIOS at BA-IFERC**

Even after implementation of the backflow model, calculation time for the DEMO divertor simulation is still much longer than that for JT-60U and JT-60SA. One of the reason is the large machine size, which makes trajectory of the MC test particles longer. Another reason is the large impurity radiation power. In the MC calculation for the large impurity radiation power, the impact of the MC noise on the plasma solution becomes large, and then the SONIC calculation becomes unstable. For stable calculation, large number of the test particles and small time step are required.

In order to accelerate simulation study for DEMO divertor design, the SONIC suite has been optimized on HELIOS super computer system at IFERC<sup>1</sup> Aomori Japan. In the SONIC suite, MC parts of NEUT2D and IMPMC can be accelerated on the many cores of HELIOS, while a fluid part SOLDOR becomes bottleneck in the iterative calculation of SONIC. Therefore, OpenMP technique is employed to the SOLDOR part, and then parallelization efficiency of the iterative calculation of SONIC is improved by ~ 20%. On Fujitsu PRIMERGY BX900 (JAEA at Tokai), the typical SONIC simulations for DEMO divertor have been carried out with 55,600 test particles. To obtain the steady-state solution, 27 hours with 64 cores were used. On the other hand, on HELIOS, the calculation time for typical calculation is decreased to about 12 hours with 1024 cores although number of the test particles increases to 340,000.

Optimization on HELIOS allows wide-range parameter survey, such as optimization of the divertor geometry, impurity species, gas-puffing etc, with stable calculation.

**(iii) development of MPMD parallel computing system**

In the DEMO divertor design study, consistency with the high performance burning plasma is important issue. High impurity radiation fraction and the resultant high impurity concentration may become problem for degradation of the core plasma confinement and the fuel dilution. Therefore, the consistent analysis using an integrated code of the core transport and the divertor transport is necessary.

In development of the integrated code, maintainabil-

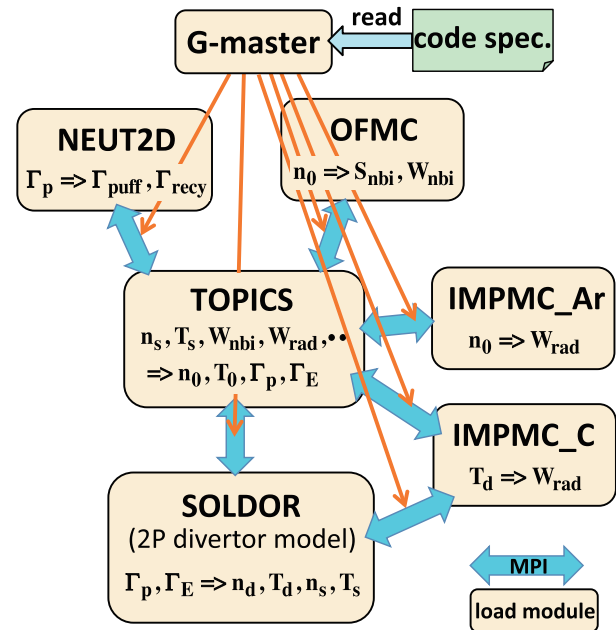


Fig. 2 The MPMD programming model for the integrated simulation.

ity of the integrated code is important because each code is maintained/improved independently. A substantial change to the integrated code is not allowed without understanding the whole code structure, especially global variable. One of solutions for such a problem is Multi-Program Multi-Data (MPMD) parallel computing system [17]. In the MPMD system, an integrated simulation can be carried out by multiple modules with data exchange via Message Passing Interface (MPI). Independence of each module is almost kept and therefore model improvement or implementation of new model become possible with small effort. The MPMD system has been already introduced to the integration of the SONIC suite and the 1.5 D core transport code TOPICS [18–20] and the time evolution of the L-H transition has been successfully simulated self-consistently [21, 22].

Recently, the MPMD system has been improved mainly in the viewpoint of the data exchange method and restructuring of the SONIC suite, i.e., SOLDOR/NEUT2D/IMPIC, on the new MPMD system is ongoing. Introduction of the MPMD system to SONIC allows implementation of a new model with a small effort: e.g. extend to multi impurity species by several IMPIC modules for He, Ar and W.

Figure 2 shows an example of the MPMD programming model for the integrated simulation. Here, the various physics model, such as SOLDOR, NEUT2D, IMPIC, TOPICS etc, are simulated by a simple model instead of the actual codes. The integrated code contains various physical interactions between modules, as shown in Fig. 2. For example, the core transport module TOPICS requires various parameters from the other module, such as, temper-

<sup>1</sup>International Fusion Energy Research Centre under the Broader Approach collaboration between Euratom and Japan

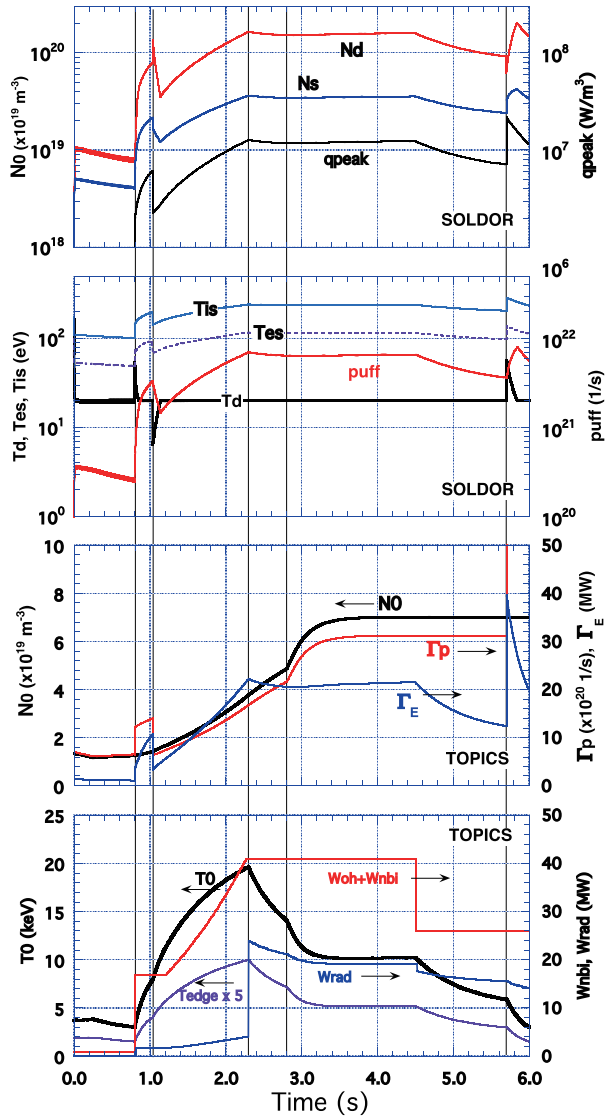


Fig. 3 Integrated simulation for the controllability of temperature at the divertor plate by the gas puffing.

ature and density at the mid-plane, the recycling flux from divertor, impurity radiation power, heating power and so on. On the other hand, such input data from several modules strongly depends on the core transport. In the MPMD system, each model works independently and only necessary data is directly exchanged between models via MPI.

The MPMD integrated simulation for the controllability of temperature at the divertor plate are carried out as a demonstration. The time evolution of the physics parameters is shown in Fig. 3. The NB heating starts at  $t = 0.8$  s and the L-H transition occurs at  $t \sim 1.0$  s. (In the simple model, the L-H transition is simulated by artificial increase in the confinement time at  $T0 > 0.8$  keV.) At the time, the divertor density and temperature drop. With increasing the particle and power exhaust flux from the core ( $I_p$ ,  $I_E$ ) and the NB heating power  $W_{nib}$ , the divertor density  $Nd$  and the SOL density  $Ns$  and temperature  $Ts$  increase gradually and then, they reach the steady state. During the operation,

the divertor temperature  $Td$  is controlled to keep 20 eV by feedback of the fuel gas puffing. As just described, on the MPMD system, individual models can collaboratively simulate discharge scenario containing various physical interactions

### 3. Design Study of DEMO Divertor Plasma

As was mentioned in section 1, the huge power of larger than 500 MW must be handled in the SOL and divertor region. For the power handling, the basic concept of the divertor geometry in SlimCS is similar to that of ITER, i.e., formation and control of detachment of the divertor plasma. In SlimCS, effects of the divertor geometry on the power and particle handling are enhanced from ITER concept: (1) longer divertor leg and larger inclination of the target than those in ITER to increase particle recycling near the strike point and radiation power efficiently, (2) a larger private dome to increase the neutral pressure for exhaust of tritium gas and helium ash from the private flux region, (3) the V-shaped corner at the outer divertor to produce plasma detachment efficiently.

In this section, recent simulation studies for the DEMO divertor design are summarized.

#### 3.1 Power handling by Ar impurity Seeding

The power handling in the SlimCS divertor plasma using the Ar seeding have been investigated by using the SONIC suite [10–13]. The numerical setup for the SONIC simulation is as follows: at the core interface boundary ( $r/a \sim 0.95$ ), the deuterium ion density  $n_D^{cib}$  is fixed to  $n_D^{cib} = 7 \times 10^{19} \text{ m}^{-3}$  and the total exhausted power  $P_{cib} = P_{ext}$  is set to be 500 MW, which corresponds to  $P_{fus} = 3 \text{ GW}$ . For simplification of the SONIC simulation, only  $D^+$  ion is taken into account as fuel. The anomalous transport coefficients for the particle ( $D_{\perp} = 0.3 \text{ m}^2/\text{s}$ ) and heat ( $\chi_{\perp}^i = \chi_{\perp}^e = 1.0 \text{ m}^2/\text{s}$ ) are assumed to be spatially constant, and the same as the ITER simulation [23]. A total fuel gas puff of  $\Gamma_{puff} = 1.0 \times 10^{23} \text{ atom s}^{-1}$  ( $\sim 200 \text{ Pa m}^3 \text{ s}^{-1}$ ) is injected as molecular flux from the outer divertor and the outer midplane. The recycling on the first wall and the divertor target is assumed to be 100%, and the effective pumping speed of  $S_{pump} = 200 \text{ m}^3 \text{ s}^{-1}$  is specified at the pumping port. The location of the gas puff and the pumping port are shown in Fig. 1. The impurity gas is injected from the outer divertor to reduce the divertor heat load. The gas puff rate is adjusted by a feedback to achieve the total impurity radiation power of  $P_{rad}^{tot} = 460 \text{ MW}$  ( $P_{rad}^{tot}/P_{cib} = 0.92$ ).

The total Ar impurity radiation power increases to 460 MW by the Ar gas puffing of  $1.43 \times 10^{21} \text{ s}^{-1}$ . As shown in Fig. 4, large radiation power density is seen along the separatrix. The radiation power in the inner and outer divertor regions are  $P_{rad}^{div} = 127 \text{ MW}$  and  $P_{rad}^{odiv} = 180 \text{ MW}$ , respectively. The radiation power at the upstream, i.e., in

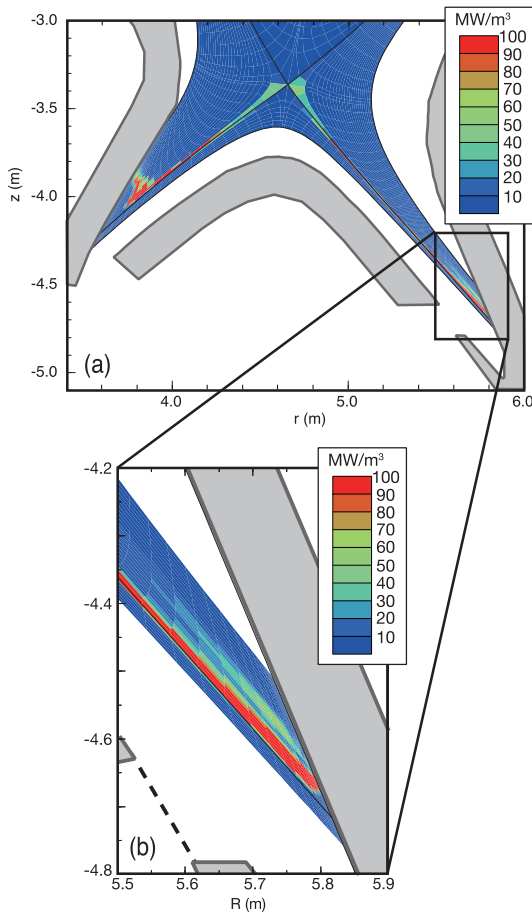


Fig. 4 Spatial profile of the Ar impurity radiation density (a) in the divertor region and (b) closeup of the outer target.

the edge region ( $0.95 < r/a < 1.0$ ) and the SOL region  $P_{\text{rad}}^{\text{edge+SOL}}$  is 153 MW ( $P_{\text{rad}}^{\text{edge+SOL}}/P_{\text{ext}} = 0.31$ ).

In the outer divertor, by the large impurity radiation along the separatrix, the partial detachment, i.e.,  $T_e$  and  $T_i$  less than 2 eV, is produced near the strike point ( $d_{\text{sp}} \leq 5$  cm), as shown in Fig. 5 (a). On the other hand, at  $d_{\text{sp}} > 5$  cm,  $T_e$  and  $T_i$  increase and the divertor plasma is still attached. The difference of  $T_e$  and  $T_i$  is enhanced due to the low  $n_i$  and low collisionality. Low amplification of fuel and impurity recycling may be caused by the inclined target.

The target heat load,  $q_d$ , is evaluated by  $q_d = \gamma n_d C_{\text{sd}} T_d + n_d C_{\text{sd}} E_{\text{ion}} + q_d^{\text{rad}} + q_d^{n_0}$ , where  $\gamma$ ,  $n_d$ ,  $C_{\text{sd}}$ ,  $T_d$ ,  $E_{\text{ion}}$  are the sheath transmission coefficient, the density, the plasma sonic speed, the temperature at the divertor sheath, the ionization energy, respectively. The first and second terms correspond to the heat load transported by convection and conduction of electrons and ions ( $q_d^{\text{plasma}}$ ), and the ionization energy released by the surface recombination of the ion flux at the target  $q_d^{\text{rec}}$ , respectively. The third  $q_d^{\text{rad}}$  and fourth  $q_d^{n_0}$  terms are radiation power from the divertor plasma, and neutral flux due to charge exchange and volume recombination, respectively. Here, in estimation of  $q_d^{\text{rad}}$ , the reflection of the photon energy on the wall surface and the absorption of the photon in the neutrals are

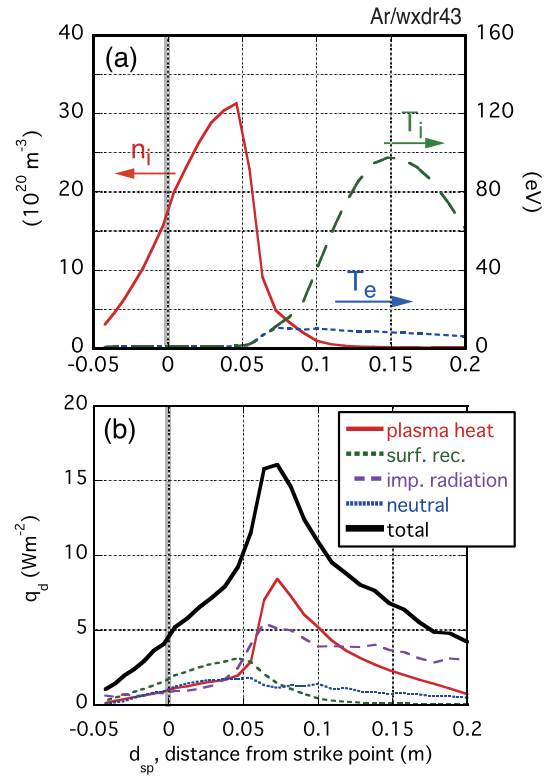


Fig. 5 Radial profiles of (a)  $n_i$ ,  $T_e$  and  $T_i$ , and (b) the target heat load.

neglected. The target heat load is shown in Fig. 5 (b). The plasma heat load  $q_d^{\text{plasma}}$  decreases to less than 8 MW/m<sup>2</sup> due to the partial detachment. In the attached region,  $q_d^{n_0}$  is less than 1 MW/m<sup>2</sup>, while it increases to 2–3 MW/m<sup>2</sup> in the detached region. As shown in Fig. 4 (b), large impurity radiation power is seen close to the target, and the radiated power becomes the target heat load  $q_d^{\text{rad}}$ . Large  $q_d^{\text{rad}}$  of 4–5 MW/m<sup>2</sup> can be seen over the wide target area. Consequently, peak of the total target heat load becomes 16 MW/m<sup>2</sup> although the 92% of the exhausted power is radiated by the Ar impurity.

### 3.1.1 Effect of seeded impurity species

Large impurity radiation close to the target, as shown in Fig. 4, is not preferable for the target heat load. Therefore, large radiation loss over the wide plasma region such as the main SOL and edge as well as the divertor is required in the DEMO reactor. Higher Z impurity will be preferable since radiation loss rate coefficient for higher Z impurity is increased at high  $T_e$ . Effects of seeding impurity species (Ne, Ar and Kr) on detachment and radiation distribution are compared.

Distributions of the radiation power density for Ne and Kr seeding cases are shown in Figs. 6 (a) and (b), respectively. For the low Z impurity (Ne), strong radiation is seen along the separatrix similar to that for the Ar seeding as shown in Fig. 4. With increasing Z (Ar and Kr), width of the intense radiation area above the target is

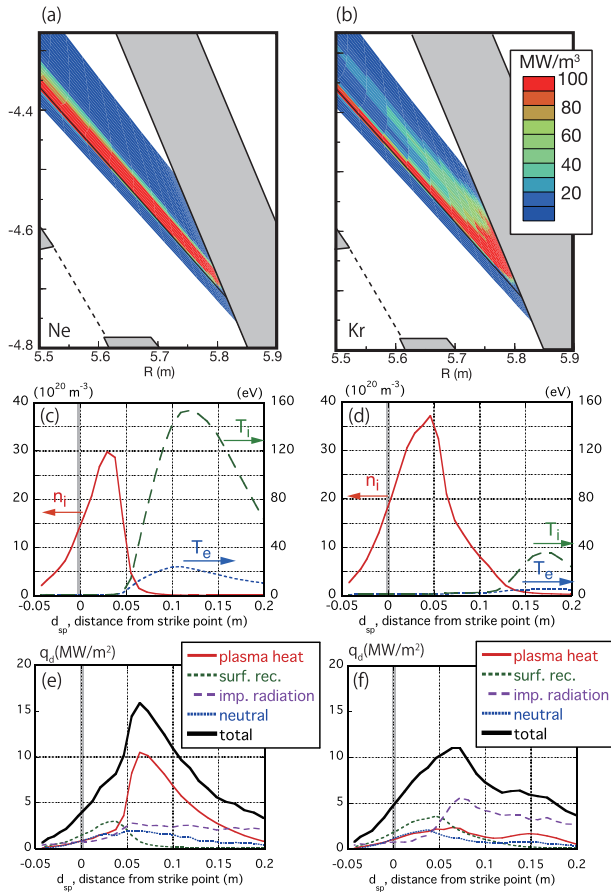


Fig. 6 Spatial profile of the impurity radiate power and the radial profile of  $N_i$ ,  $T_i$ ,  $T_e$  and  $q_d$  for Ne (left) and Kr (right).

gradually increased. For the Ne seeding case,  $P_{\text{rad}}^{\text{div+odiv}} = 374 \text{ MW}$  (75 % of  $P_{\text{ext}}$ ) is significantly larger than  $P_{\text{rad}}^{\text{edge+sol}}$  of 87 MW (17 %). On the other hand, for the Kr seeding case,  $P_{\text{rad}}^{\text{edge+sol}}$  is increased to 229 MW (46 %) while  $P_{\text{rad}}^{\text{div+odiv}}$  is decreased to = 230 MW (46 %).  $P_{\text{rad}}^{\text{edge+sol}}$  and  $P_{\text{rad}}^{\text{div+odiv}}$  become comparable. Here, in the inner divertor,  $P_{\text{rad}}^{\text{div}}$  is reduced with higher Z and the large radiation area moves further upstream.

Profiles of the outer divertor plasma and heat load for Ne and Kr seeding cases are shown in Figs. 6 (c) - (f). Since the radiation loss is enhanced near the separatrix for the low Z impurity (Ne), the plasma detachment is produced in the relatively narrow region near the strike-point ( $d_{\text{sp}} < 4 \text{ cm}$ ). The peak  $q_d$  of  $16 \text{ MW/m}^2$  is seen at the boundary of the detachment, and it is similar to that for the Ar seeding case. With increasing Z, profile of the intense radiation area extends widely above the target, and width of the partial detachment region is increased to  $d_{\text{sp}} \sim 5 \text{ cm}$  (Ar) and  $10 \text{ cm}$  (Kr). For the Kr seeding, peak  $q_d$  is decreased to  $11 \text{ MW/m}^2$  due to a large reduction in  $q_d^{\text{plasma}}$  ( $= 2.3 \text{ MW/m}^2$ ), while  $q_d^{\text{rad}}$  ( $= 5.6 \text{ MW/m}^2$ ) and  $q_d^{\text{no}}$  ( $= 2.1 \text{ MW/m}^2$ ) are similar to those for the Ar seeding case.

Consequently, distribution of the radiation power can be controlled by selecting the impurity seeding gas. With increasing Z,  $P_{\text{rad}}^{\text{edge+sol}}$  becomes comparable to  $P_{\text{rad}}^{\text{div+odiv}}$ ,

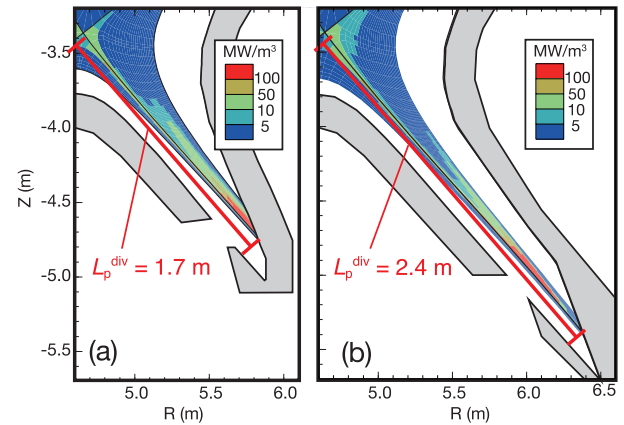


Fig. 7 Divertor geometry for the reference case (original geometry of the SlimCS divertor) and (b) the long-leg case, and spatial profiles of the Ar impurity radiation power.

and the wider plasma detachment and lower peak  $q_d$  can be produced in the outer divertor. The peak  $q_d$  is still larger than the divertor power handling capability even for the case of Kr, further improvement of the power handling is necessary.

### 3.1.2 Geometry effect

The divertor geometry plays an important role for the detachment formation and control of the radiation distribution. Divertor design with a V-shaped corner was efficient to enhance fuel and impurity recycling near the strike-point, and to produce the partial detachment [10]. Divertor plasma temperature  $T_d$  is expected to decrease in long divertor leg because  $T_d \propto q_{\parallel}^{10/7} n_u^{-2} (L_{\parallel}^d)^{-4/7}$  is decreased with increasing the connection length to the target ( $L_{\parallel}^d$ ) from a simple 2-point model, where  $q_{\parallel}$  and  $n_u$  are the parallel heat flux and the upstream plasma density, respectively.

The effect of the divertor leg length is investigated. The divertor geometry for the reference (original geometry of the SlimCS divertor) and long-leg divertors are compared in Fig. 7. The size of the long-leg divertor, i.e. poloidal length from the divertor null to the target  $L_p^{\text{div}}$ , is increased from 1.7 to 2.4 m (1.4 times longer). This corresponds to increase in  $L_{\parallel}^d$  by 14 %. Since the magnetic configuration is kept, the magnetic flux expansion at the target is reduced to 67 % with increase in the divertor-leg and the wetted area ( $A_{\text{wet}}$ ) is decreased to 63 %.

Figure 8 (a) shows the radial profiles of the divertor plasma. Due to increase in the divertor-leg,  $T_i$  and  $T_e$  are decreased and therefore the divertor recycling is enhanced. In addition, the deeper V-shaped corner also enhances the divertor recycling. Consequently, both  $T_i$  and  $T_e$  are decreased to less than 2 eV over the target, i.e., the full detachment is produced in the long-leg divertor. The large radiation area moves upstream and clearly separates from the target, as shown in Fig. 7.

Due to the full detachment in the long-leg divertor,

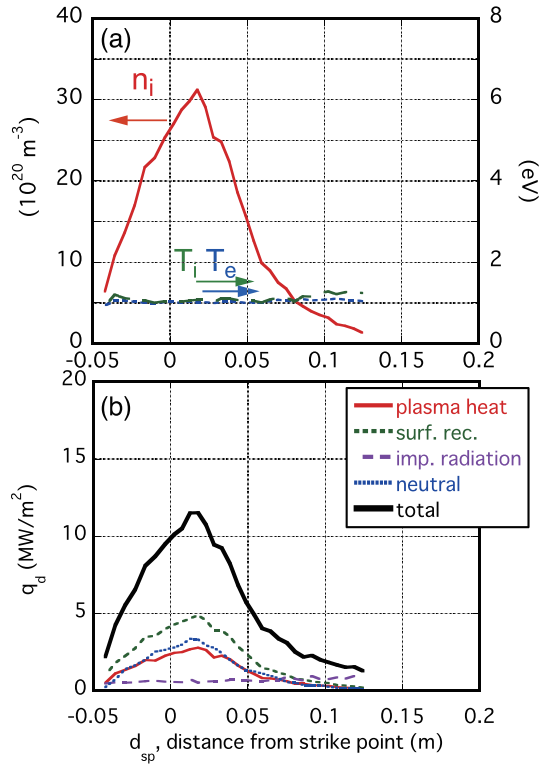


Fig. 8 Radial profile of the divertor plasma and the heat load on the outer target in the long-leg divertor.

heat loads by the plasma transport and radiation are significantly reduced to  $2.8 \text{ MW/m}^2$  and  $0.9 \text{ MW/m}^2$ , respectively. On the other hand, components due to surface recombination and neutral flux are increased to  $4.9 \text{ MW/m}^2$  and  $3.4 \text{ MW/m}^2$ , respectively, as shown in Fig. 8 (b). This may be caused by the smaller magnetic flux expansion in the long-leg divertor. Consequently, peak  $q_d$  decreases to  $11.5 \text{ MW/m}^2$  from  $16 \text{ MW/m}^2$  in the reference case. Optimization of the divertor geometry and enhancement of the dissipation of the ions and neutrals will be required to reduce the peak heat load.

In the long-leg divertor,  $P_{\text{rad}}^{\text{odiv}}$  is significantly enhanced to  $280 \text{ MW}$  (56% of  $P_{\text{ext}}$ ). Both  $P_{\text{rad}}^{\text{div}}$  and  $P_{\text{rad}}^{\text{edge+sol}}$  become smaller, i.e.,  $P_{\text{rad}}^{\text{div}} \sim P_{\text{rad}}^{\text{edge+sol}} \sim 90 \text{ MW}$  (18%). As a result,  $P_{\text{rad}}^{\text{div}}$  is increased from  $307 \text{ MW}$  (61% of  $P_{\text{ext}}$ ) to  $370 \text{ MW}$  (74% of  $P_{\text{ext}}$ ).

This result means that the radiation distribution at the main edge / divertor and the target heat load can be controlled by the divertor geometry as well as the seeding impurity species.

### 3.2 Impact of the fusion power

The power handling is one of the most critical issue for the DEMO design. Therefore, change of the machine specification, such as the fusion power, the machine size and so on, may be necessary for the divertor power handling.

To solve the power handling issue and to explore the

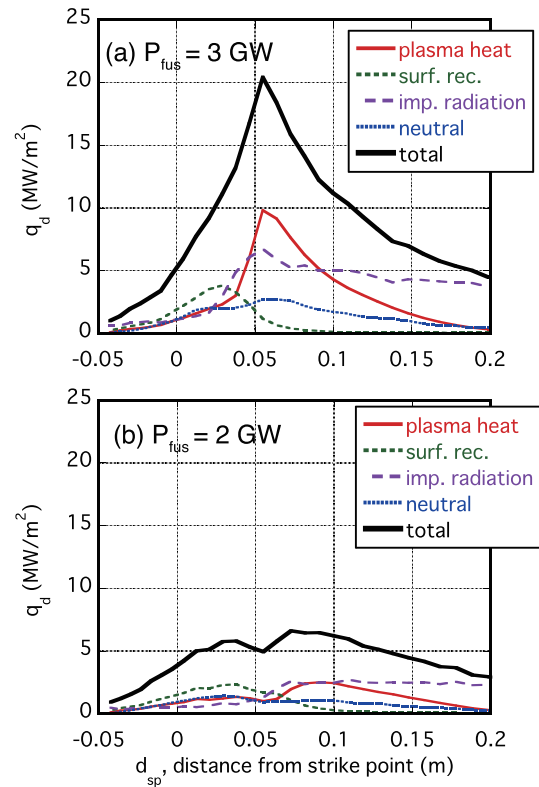


Fig. 9 Comparison of the target heat load profile between the  $P_{\text{fus}} = 3 \text{ GW}$  and  $2 \text{ GW}$  cases.

operational window from the viewpoint of the power handling, impact of fusion power on the divertor performance are investigated as the first step. The exhaust power across the core interface boundary is decreased from  $500 \text{ MW}$  to  $320 \text{ MW}$ , which corresponds to decrease in  $P_{\text{fus}} = 3 \text{ GW}$  to  $2 \text{ GW}$ . The impurity radiation fraction is kept to 92% in both cases. Here we should note that some numerical setup is different from the above simulations. The boundary condition for the particle at  $r/a \sim 0.95$  is changed from the fixed density in above simulations to the particle flux of  $6 \times 10^{22} / \text{s}$ . In order to reduce the calculation time, the calculation of the impurity transport is limited to 50 ms. As a result, in the 3 GW case, the mid-plane density is decreased from  $3.4 \times 10^{19} \text{ m}^{-3}$  to  $2.9 \times 10^{19} \text{ m}^{-3}$  and the peak target heat load increased from  $16 \text{ MW/m}^2$  (previous result) to  $20 \text{ MW/m}^2$ .

In  $P_{\text{fus}} = 2 \text{ GW}$  case, the ion and electron temperature at the target is decreased as expected by a simple 2-point model  $T_d \propto q_{\parallel}^{10/7} n_u^{-2} (L_{\parallel}^d)^{-4/7}$ . Then the recycling is enhanced and the detached region is extended. Comparison of the target heat load profile is shown in Fig. 9. Due to enhancement of the detachment, the plasma heat load significantly decreases. At the same time,  $T_e$  in the 2 GW case decreases also in the poloidal direction. Therefore, the impurity radiation region slightly moves upstream and the radiate load is also decreased. Consequently, the peak target heat load significantly decreases from  $20 \text{ MW/m}^2$  to  $6.6 \text{ MW/m}^2$ .

## 4. Summary and Future Work

In the DEMO reactor at the fusion power of 3 GW, the huge exhausted power of more than 500 MW must be handled in the divertor, SOL and edge region. Huge power handling in the SOL/divertor region is one of the most crucial issues for a tokamak fusion reactor. In JAEA, divertor design study of a DEMO reactor has been progressed using a suite of integrated divertor codes SONIC.

In order to obtain the stable solution for the DEMO divertor plasma simulation, the SONIC suite has been improved. The conversion of solution was improved and the calculation time was decreased by (i) introducing of the backflow model for the simplified impurity exhaust process and (ii) optimization on HELIOS super computer at BA-IFERC. In addition, toward self-consistent analysis of the high performance burning plasma and the divertor power handling, development of the integrated simulation is in progress by using the MPMD parallel computing system.

The SONIC simulation has demonstrated that the partial detached divertor plasma was achieved by the Ar impurity seeding to radiate 92 % of the exhaust power. Although the heat load due to the plasma heat transport was significantly reduced due to the partial detachment, the contribution of the impurity radiation and the surface recombination of the fuel ions to the target heat load became large. As a result, the peak of the total divertor heat load was estimated to be 16 MW/m<sup>2</sup>. In order to reduce the total heat load, controllability of the impurity radiation distribution by kind of seeding impurity species and the divertor geometry has been investigated. They can decrease the target heat load, but the further design study is still necessary to reduce the target heat load to the power handling capability for a tungsten mono-block divertor with water cooling. To solve the divertor power handling issue and to explore the operational window, impact of the fusion power on the power handling has been studied. Decrease in the fusion power can reduce the target heat load mainly due to the enhancement of the detachment.

In the future work, improvement of the divertor geometry including the magnetic configuration as well as plasma operation will be necessary for not only reduction of the target heat load but also reduction of the impurity radiation fraction. In this study, the divertor simulation has been performed with impurity radiation fraction of more than 90 %, but it is difficult to extrapolate from the existing experiments accompanied by the energy confinement and

fuel dilution appropriate for the reactor plasmas.

Further improvement and development of the SONIC code such as detachment of the ion flux, SOL plasma flow, drift effects and kinetic effects in impurity transport, etc., are necessary. Development of the integrated simulation including the impurity transport in the core region is in progress to analyze the integrated performant of the high performance burning plasma and the divertor power handling.

## Acknowledgement

This study, especially code development, was partially supported by Grants-in-Aid for Scientific Research of Japan Society for the Promotion of Science. The work is mainly carried out within the framework of the BA DEMO Design Activity. A part of numerical simulation was performed using the HELIOS supercomputer system at BA-IFERC, implemented by Fusion for Energy and Japan Atomic Energy Agency.

- [1] M. Kikuchi *et al.*, Fusion Eng. Des. **16**, 253 (1991).
- [2] R. Hiwatar *et al.*, Nucl. Fusion **45**, 96 (2005).
- [3] F. Najimabadi *et al.*, Fusion Eng. Des. **80**, 3 (2006).
- [4] K. Lackner *et al.*, J. Nucl. Mater. **307**, 10 (2002).
- [5] D. Maisonnier *et al.*, Nucl. Fusion **47**, 1524 (2007).
- [6] K. Tobita *et al.*, Nucl. Fusion **47**, 892 (2007).
- [7] K. Tobita *et al.*, Nucl. Fusion **49**, 075029 (2009).
- [8] K. Kawashima *et al.*, Plasma Fusion Res. **1**, 031 (2006).
- [9] K. Shimizu *et al.*, Nucl. Fusion **49**, 065028 (2009).
- [10] H. Kawashima *et al.*, Nucl. Fusion **49**, 065007 (2009).
- [11] N. Asakura *et al.*, J. Plasma Fusion Res. SERIES **9**, 136 (2010).
- [12] K. Hoshino *et al.*, Contrib. Plasma Phys. **52**, 550 (2012).
- [13] N. Asakura *et al.*, Nucl. Fusion **53**, 123013 (2013).
- [14] R. Schneider *et al.*, Contrib. Plasma Phys. **46**, 3 (2006).
- [15] T.D. Rongnlien *et al.*, J. Nucl. Mater. **196-198**, 347 (1992).
- [16] K. Hoshino *et al.*, Contrib. Plasma Phys. **54**, 404 (2014).
- [17] A. Takayama *et al.*, J. Plasma Fusion Res. SERIES **9**, 604 (2010).
- [18] N. Hayashi *et al.*, Nucl. Fusion **49**, 095015 (2009).
- [19] T. Ozeki and JT-60 Team, Phys. Plasmas **14**, 056114 (2007).
- [20] N. Hayashi and JT-60 Team, Phys. Plasmas **17**, 056112 (2010).
- [21] K. Shimizu *et al.*, 23rd Fusion Energy Conference (Daejeon, Korea, 2010), Contributed Papers, THD/5-2Ra (IAEA, Vienna) <http://www-pub.iaea.org/mtcd/meetings/cn180/papers.asp>
- [22] M. Yagi *et al.*, Contrib. Plasma Phys. **52**, 372 (2012).
- [23] A.S. Kukushkin *et al.*, J. Nucl. Mater. **337-339**, 50 (2005).